

Emission Spectroscopy of the Combustion Flame of Aluminium/Copper Oxide Thermite

Sebastian Knapp,^{*,[a]} Stefan Kelzenberg,^[a] Angelika Raab,^[a] Evelin Roth,^[a] and Volker Weiser^[a]

Abstract: The combustion process of stoichiometric aluminium/copper(II)oxide thermite was experimentally investigated in an optical bomb under inert atmosphere (N_2) and ambient pressure. The reaction zone was monitored with UV/VIS emission spectroscopy and a colour high-speed camera. The emission spectra were analysed by modelling of the background radiation and the characteristic emission of all molecular emitters in the reaction of Al/CuO. Based on

this, the particles' surface and gas phase temperature, the emissivity and the radiation of energy was determined by a non-linear least squares fit between experimental and modelled spectra. This work presents the first modelling of the diatomic band system of Cu_2 and CuO. The results obtained can help to understand the underlying processes in thermite combustion and the influence of radiation processes in modelling the combustion of thermite mixtures.

Keywords: Emission • Thermite • Combustion • UV/VIS-spectroscopy

1 Introduction

Thermite type reactions – in which a metal is oxidized by a metal-oxide to form a more stable metal-oxide and a metal or alloy from the oxide – are highly exothermic chemical reactions. Those reactions belong to the group of solid state reactions, because the educts and products are mostly in the solid phase. Thermite reactions are applied to achieve high temperature and high thermal energy release [1]. Thermite reactions were first described in 1898 by Goldschmidt and Vautin as a “carbon-free” method to extract metals by reducing their oxides with aluminium [2]. This type of reaction is of widespread interest to rapidly produce large amounts of heat at high temperature levels and has found many applications. The thermite welding process is the main method for welding of railroad tracks [3]. Its many variations are also used to produce all kinds of metal powders, composite materials and refractory ceramics [4–9]. Due to the large heat release and the self-sustaining nature of their combustion, thermites have been used in warheads as incendiary devices [10,11]. A big advantage of most thermite compositions based on micrometric components is that they are not very sensitive towards friction, impact shock and particularly ESD.


Thermites composed from aluminium and copper(II) oxide have interesting combustion properties because of the intermediate vaporization of copper formed by the reduction of CuO [12]. Nanometric types of this thermite are predominantly investigated for different applications [13] because of higher burning rates [14–16]. Mostly, the disadvantage of higher sensitivity in comparison to micrometric thermites [17] and the problems resulting from the occupational and environmental impact of nano-materials

[18] is accepted. Therefore, new preparation methods are the subject of ongoing research [19,20].

Flame Spectroscopy is often used for the identification of atoms and molecules in the combustion zone of thermites [21]. Due to the high reaction temperatures, transient reaction products can be present in the vapour phase. This is confirmed by emission spectra showing band systems of intermediate products and is shown e.g. in Ref. [22]. In the case of aluminium/copper(II) oxide thermite reaction, research has been reported in [23] and [24] also focused on nano-thermites and the determination of relative intensities and temperature determination by grey body radiation.

In the present work, the condensed phase temperature was determined by calculating the grey body radiation of the background. Furthermore, the spectra of intermediate diatomic species and the reaction zone temperature of the Al/CuO thermite reaction were investigated. The spectroscopic properties of the gaseous diatomic copper compounds Cu_2 and CuO were calculated for the first time and the results of the vibrational overlap integral (Franck-Condon factors) are presented. The temperatures were determined by comparison of calculated with experimental spectra by a non-linear least squares fit. The final outcome will help to understand the involved processes in thermite combustion and to integrate the radiation processes in modelling of thermite mixtures [25–27].

[a] S. Knapp, S. Kelzenberg, A. Raab, E. Roth, V. Weiser
Energetic Systems
Fraunhofer Institute for Chemical Technology ICT
Joseph-von-Fraunhofer-Straße 7, 76327 Pfinztal, Germany
*e-mail: sebastian.knapp@ict.fraunhofer.de

 Supporting information for this article is available on the WWW under <https://doi.org/10.1002/prep.201800235>

2 Experimental

Al/CuO (Toyol Europe: Alcan 400, 99.7% min., Aluminium powder atomized; Alpha Aesar: Copper(II) oxide, 97%, –325 mesh powder) particles were mixed for one hour in a tumbling mixer. The thermite mixtures were burned in a high pressure autoclave ignited by a hot wire with a small booster-mixture. The thermite samples were burned as a small pile (2 mm × 4 mm × 15 mm) of bulk material of about 1 g in a 0.1 MPa nitrogen atmosphere (purity 99.999% (4.9)). On the two windows of the bomb, a UV/Vis emission spectrometer (Andor: Shamrock SR-500i, Newton DU920P-UV-BR-DD) via an optical quartz lens system and a colour high-speed camera (Redlake: MotionPro X3) were adapted. Additionally an NIR spectrometer (Zeiss: MCS 621 Vis2/MCS 611 NIR 2.2) was adapted by an optical fibre. The optical lens system makes a 1:1 transformation of the measurement point (selected by the aperture B1) to the entrance slit of the spectrometer. The experimental setup is shown in Figure 1.

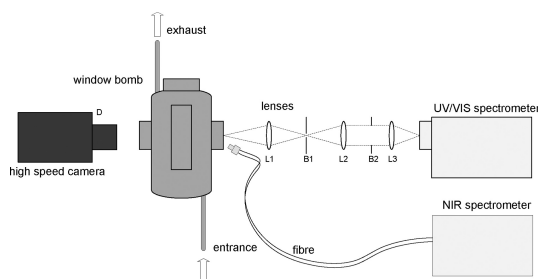


Figure 1. Schematic sketch of the experimental setup.

3 Modelling

3.1 Grey Body Radiation

Thermite reactions produce hot particles and glowing solid particles with temperatures above $T=2000$ K, which emit continuous radiation [28]. For the modelling of their emission, a grey body radiation is assumed [29], which is described by Planck's law with a wavelength and temperature independent emission coefficient. At these high temperatures the peak maximum of the grey body radiation is in the NIR-range at $\lambda_{\max}=1.4489 \mu\text{m}$ (2000 K; according to Wien's displacement law: $\lambda_{\max} = \frac{2897.8 \mu\text{m K}}{T}$) but a part of the grey body radiation is also visible in the UV/VIS range as background. Due to the optical setup the emissivity of the measurement point can be determined which depends on the concentration and size of the emitting particles. From there the total radiance can be approximated by the Stefan-Boltzmann law of radiation.

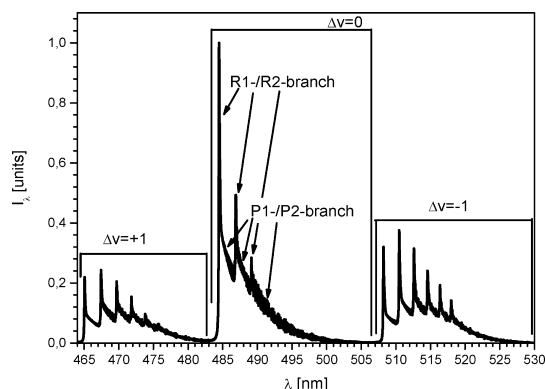


Figure 2. Calculated emission spectrum of AlO molecule $B^2\Sigma-X^2\Sigma$ transition.

3.2 Diatomic Molecule Spectrum

In addition to the background (grey body) radiation during thermite reaction, electronically excited atoms and diatomic molecules in the reaction zone emit their characteristic lines and band systems [30]. The underlying species (atoms and molecules) can be identified by tabulated data from literature [31] and the spectra calculated based on quantum mechanical principles [32]. Solving the Schrödinger equation using the Born-Oppenheimer approximation provides the energy, respectively wavelength; the Einstein coefficients for spontaneous emission provide the transition probabilities (dipole moments) and intensities. Together with a line profile a spectrum of a diatomic molecule can then be calculated. Detailed information is given in the supporting information or in [32, 33].

3.3 AlO

In the combustion flame of the Al/CuO thermite, the $B^2\Sigma-X^2\Sigma$ -band system of AlO is observed. For both states, excited and ground state, Hund's coupling case b is valid and the expression for the rotational energy split by spin-rotation interaction is given by [34]:

$$F_{v,e}(J) = B_v J(J+1) - D_v J^2(J+1)^2 + \frac{\gamma}{2} \left(J - \frac{1}{2} \right) \quad (1)$$

$$F_{v,f}(J) = B_v J(J+1) - D_v J^2(J+1)^2 - \frac{\gamma}{2} \left(J + \frac{1}{2} \right) \quad (2)$$

with the electron spin-rotation coupling constant γ . The molecule constants were taken from the literature [35, 36]. The Franck-Condon-Factors needed for the calculation of the transition probabilities of the vibrational levels are from Ref. [37]. The Hönl-London-Factors are given in the supporting information. They were taken from [38–40]. Figure 2 shows a calculated emission spectrum of AlO at $T=3000$ K

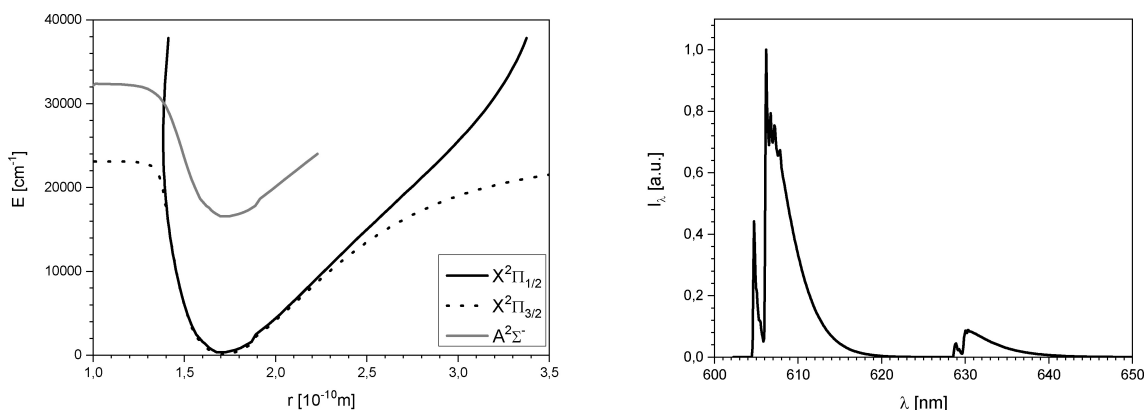


Figure 3. Calculated potential energy curves (left) and spectrum of CuO molecule $A^2\Sigma-X^2\Pi_{3/2}$ transition at 3000 K (right).

which appears in the wavelength range between $\lambda = 465$ –530 nm.

$$S_J^P = J \quad S_J^Q = 0 \quad S_J^R = J + 1 \quad (3)$$

3.4 CuO

Besides the bands for AlO the spectrum also shows bands for CuO in the combustion flame. The $A^2\Sigma-X^2\Pi$ transition of CuO is observed between $\lambda = 604$ –650 nm. The energy terms of the excited state interact in Hund's coupling case b and they are given in Eqs. (1) and (2). The ground state couples in an intermediate state between Hund's case a and b described by the coupling constant Y [41]. By the multiplicity, four energy terms result:

$$F_{1,e}(J) = B_v J \left(J + \frac{1}{2} \right)^2 - A^2 - \frac{1}{2} B_v \quad (4)$$

$$\sqrt{4 \left(J + \frac{1}{2} \right)^2 + Y(Y-4)A^2 - D_v J^2}$$

$$F_{1,f}(J) = F_{1,e}(J) + B_1 \left(J + \frac{1}{2} \right) \left(J + \frac{3}{2} \right) \quad (5)$$

$$F_{2,e}(J) = B_v J \left(J + \frac{1}{2} \right)^2 - A^2 + \frac{1}{2} B_v \quad (6)$$

$$\sqrt{4 \left(J + \frac{1}{2} \right)^2 + Y(Y-4)A^2 - D_v (J+1)^4}$$

$$F_{2,f}(J) = F_{2,e}(J) + B_1 \left(J + \frac{1}{2} \right) \left(J + \frac{3}{2} \right) \quad (7)$$

The constants were taken from the literature [42–44]. The transition probabilities of the involved vibrational states were not calculated yet. To determine them, the Franck-

Table 1. Franck-Condon factors for the $A^2\Sigma-X^2\Pi_{3/2}$ transition of CuO.

$v' \backslash v''$	0	1	2	3	4	5
0	9.46426 e-1	–	–	–	–	–
1	5.35114 e-2	8.44270 e-1	–	–	–	–
2	6.08848 e-5	1.06554 e-1	7.47021 e-1	–	–	–
3	9.40479 e-7	2.92786 e-4	1.58607 e-1	6.54659 e-1	–	–
4	6.44067 e-7	2.07044 e-6	8.60911 e-4	2.09098 e-1	5.67177 e-1	–
5	3.32672 e-8	2.91307 e-6	2.03740 e-6	1.98699 e-3	2.57389 e-1	4.84604 e-1

Condon factors were calculated from the potential energy curves. In turn, the potential energy curves were calculated by the method of Rydberg-Klein-Rees (RKR-method) using the RKR1 2.0 Code by R. J. Le Roy [45]. The method was discussed in detail in Ref. [46]. The resultant potential curves for $A^2\Sigma-X^2\Pi$ transition of CuO are shown in Figure 3 (left).

The potential energy curves and the equilibrium distances of CuO molecules were compared to literature values. They differ by a factor of two in comparison to Ref. [47]. Nevertheless, from there the Franck-Condon factors were calculated by solving the 1-dimensional Schrödinger equation with the calculated potential energy curves using the LEVEL 8.0 Code by R. J. Le Roy [48]. The vibrational transition probabilities for CuO are given in Table 1.

The Hönl-London-Factors for the transition are given by Ref [38]. With the rotational constants from [42, 44], the calculated Franck-Condon factors and a gaussian line profile, the emission bands of CuO call for a temperature of $T = 3000$ K as is indicated in Figure 3.

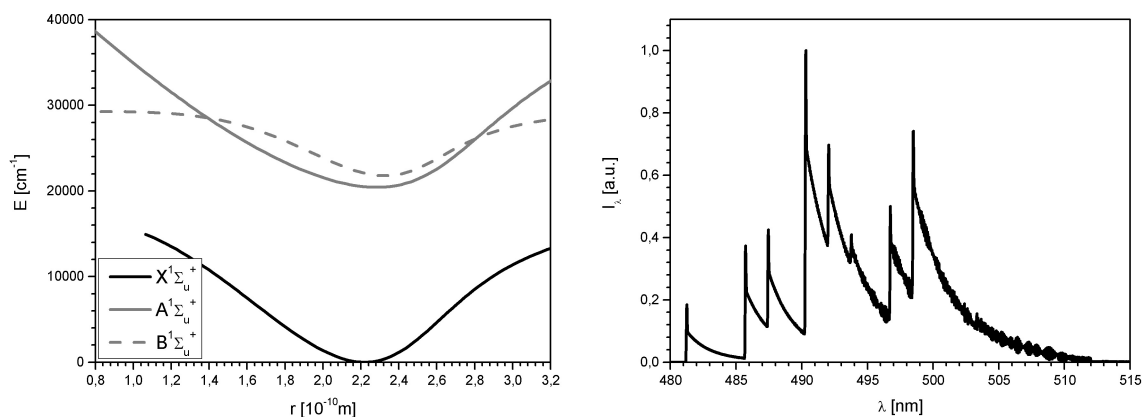


Figure 4. Calculated potential energy curves (left) and spectrum of the Cu₂ molecule A¹Σ-X¹Σ transition at 3000 K (right).

Table 2. Franck-Condon factors for the A¹Σ-X¹Σ transition of Cu₂.

v' \ v''	0	1	2	3	4	5
0	6.58143 e-01	2.13796 e-01	8.62145 e-02	2.87330 e-02	9.28075 e-03	2.77298 e-03
1	3.17659 e-01	2.43881 e-01	1.90100 e-01	1.40255 e-01	6.56741 e-02	2.76294 e-02
2	2.24293 e-02	4.73223 e-01	7.07032 e-02	1.09723 e-01	1.48270 e-01	9.26786 e-02
3	9.42308 e-04	6.28078 e-02	5.24696 e-01	1.19995 e-02	4.26660 e-02	1.26599 e-01
4	8.03881 e-04	2.65648 e-03	1.13994 e-01	5.14545 e-01	8.91042 e-05	7.20973 e-03
5	1.53435 e-07	3.50147 e-03	4.73926 e-03	1.68417 e-01	4.71815 e-01	2.23641 e-03

3.5 Cu₂

In the case of the diatomic molecule Cu₂, the A¹Σ-X¹Σ transition is visible between λ = 480–515 nm. For both states, excited and ground state, Hund's coupling case b is valid and the rotational energy levels are calculated by:

$$F(J, \Lambda) = B_e J(J+1) - (A - B_e) \Lambda^2 - D_e J^2(J+1)^2 + H_e J^3(J+1)^3 \quad (8)$$

with $\Lambda = \Sigma = 0$. The constants are from Ref. [43]. Likewise the Franck-Condon factors of the involved vibrational states for Cu₂ were not calculated yet and they were calculated by the same method described above for CuO. In Figure 4, the potential energy curves of Cu₂ are shown. The potential energy curves and the equilibrium distances of the molecule are in good agreement with Ref. [47].

The Franck-Condon-Factors of the A¹Σ-X¹Σ transition of Cu₂ are given in Table 2.

The Hönl-London-Factors are the same as the factors for the ²Σ-²Σ-transition and they are given in the supporting information. Figure 4 shows a calculated emission spectrum of Cu₂ at T = 3000 K.

3.6 Data Analysis

Besides the identification of molecular bands by comparison with literature values, the temperatures of the hot particles and surfaces and the gas phase can be determined by fitting the above described models to the experimentally measured spectra. The used fit algorithm is a non-linear least-squares fit by Powell [49] which minimizes the χ^2 -function:

$$\chi^2 = \sum_{v=1}^m f_v^2(x) \quad (9)$$

with

$$f_v = \frac{y_v - z_v(x)}{\Delta y_v} \quad (10)$$

with the measured value y_v , the theoretical value z_v and the experimental error Δy_v . The fit parameter is the temperature from Planck's law in the case of grey body emission and the intensity distribution in case of diatomic molecules. In the case of diatomic molecules, the full-width half maximum (FWHM) of each line was fixed to the FWHM of the spectrometer entrance slit.

4 Results

In Figure 5, an overview spectrum of the Al/CuO combustion in the interested wavelength range between from $\lambda = 350$ –700 nm is shown. Atomic lines of aluminium (396.2 nm), copper (570.0 nm and 578.2 nm), sodium (doublet line at 589 nm and 589.6 nm) and lithium (670.8 nm) are visible. Sodium for sure and lithium probably are pollution from aluminium production. They are the strongest lines of the involved elements in this wavelength range. They were identified by comparison with literature values [31]. By comparison with literature [31,50] and with calculated spectra, identified diatomic band systems are the AlO $B^2\Sigma-X^2\Sigma$ between $\lambda = 460$ –550 nm, the Cu_2 $A^1\Sigma-X^1\Sigma$ (480–512 nm) (see Figure 9), the $B^1\Sigma-X^1\Sigma$ system (460–480 nm) and the CuO $A^2\Sigma-X^2\Pi$ transition (604–650 nm) (see Figure 10). In the whole investigated wavelength range from 350 nm to the NIR range at $\lambda = 2100$ nm a strong background spectrum of grey body radiation appears where the atomic lines and diatomic spectra are added above.

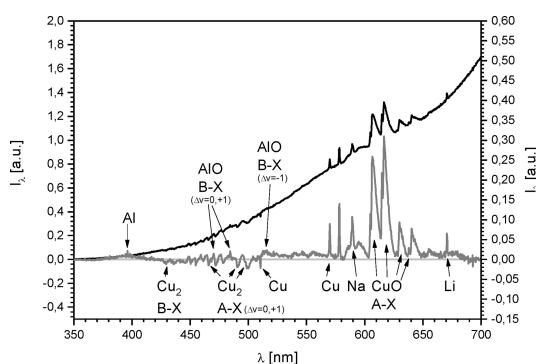


Figure 5. Overview spectra of Al/CuO thermite combustion.

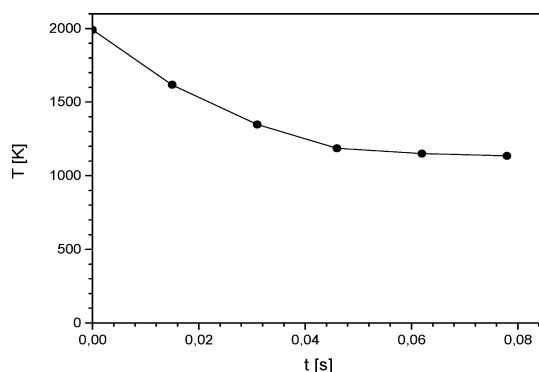


Figure 6. Determined continuum temperature in the NIR range.

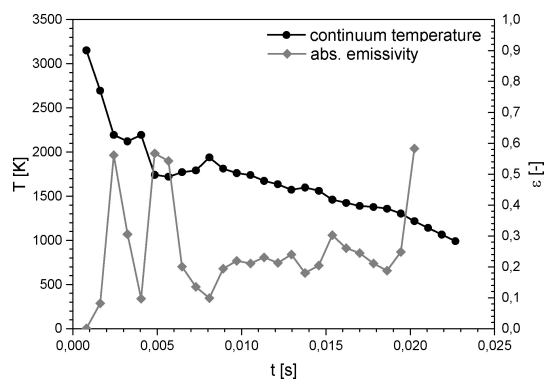


Figure 7. Determined continuum temperature and emissivity in the UV/Vis range.

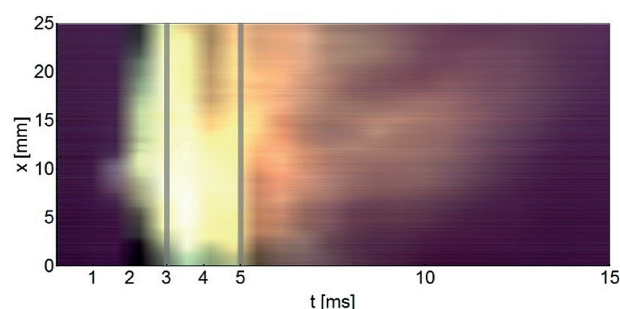


Figure 8. Result of the high-speed video: luminosity in height versus time (the sample is placed at $x = 0$ mm). The gray lines can be correlated to the first two peaks of absolute emissivity in Figure 7.

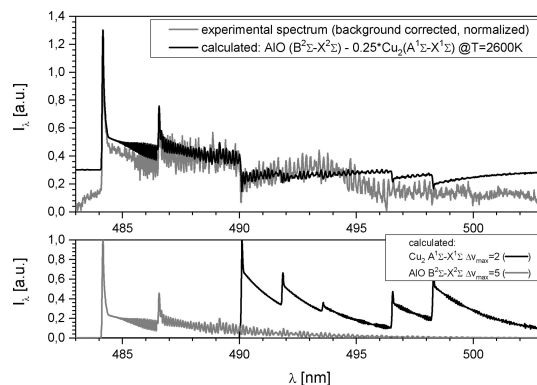


Figure 9. Illustration of the overlaying spectra of AIO and Cu_2 .

4.1 Continuum Temperatures – Absolute Calibrated Intensity

Combustion of thermites often proceeds with formation of a hot molten zone and ejection of hot particles. Both emit a grey body radiation which can be detected in the whole wavelength range from UV/VIS to NIR over to the far IR. We observed the combustion process with a VIS/NIR spectrometer and determined the temperature by a fit of a grey

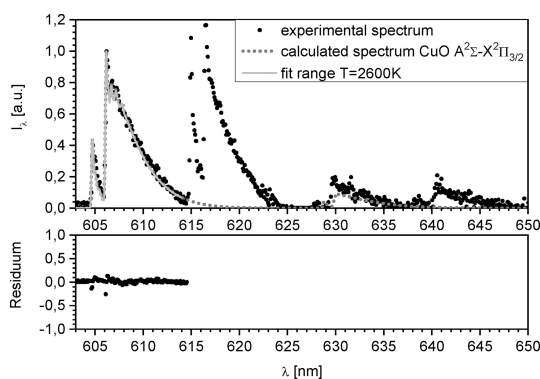


Figure 10. Fit of the calculated to an experimental spectrum of the CuO $A^2\Sigma-X^2\Pi_{3/2}$ subsystem.

body radiation function (see Figure 6). It ranges from 2000 K at the beginning till 1200 K at the end of the combustion process after 0.08 s. The process itself takes only 0.08 s because of the small sample mass. In parallel the combustion process was observed in the UV/VIS range by the emission grating spectrometer and the colour high-speed camera. The intensity of each frame of the high-speed camera video was summarized in one line and the lines were put together to a new picture. The new picture shows the integral intensity colour-coded over height (y-coordinate) and time (x-coordinate) (see Figure 8). By the optical setup described above, an absolute calibration of the spectrometer can be performed by the tungsten strip lamp. The result is intensity in units of $\text{W m}^{-2} \text{nm}^{-1} \text{sr}^{-1}$. Therefore, the absolute emissivity and the continuum temperature of the combustion process at the measurement point of the optical setup can be determined by fitting a grey body function to the experimental spectra. A result for the combustion of the Al/CuO thermite is shown in Figure 7 (black = continuum temperature, grey = emissivity). The determined emissivity is between $\varepsilon = 0.002$ at the beginning and up to 0.57 at the two peaks after $t = 2.5$ ms and 5 ms. The two peaks can additionally be correlated with the two bright strips in the analysed high-speed video picture (Figure 8).

With the continuum temperature and the emissivity, the radiated energy at the measurement point can be calculated with the Stefan-Boltzmann-Law. For calculation of the radiated energy of the whole combustion process the geometry of the flame and the temperature and emissivity at each point in the flame must be known. Determination of the temperature and emissivity profile over the whole flame is therefore a special challenge.

4.2 Gas-Phase Temperature – Comparison of Diatomic Spectra

The gas phase temperature can be determined by modelling the spectra of the observable diatomic molecule bands

and fit them to experimental one. In the case of Al/CuO thermite sometimes the $\text{Cu}_2 A^1\Sigma-X^1\Sigma$ system overlays with the AlO system or it is in absorption, so that temperature determination by fitting the calculated spectrum of Cu_2 or AlO to the experimental one is impossible (Figure 9). The overlay factor (0.25) of the calculated spectra (black line) was arbitrarily selected. The band head of the AlO $B^2\Sigma-X^2\Sigma$ system with $\Delta v = 0$ vibrational band do not overlay and for this small wavelength range from 483.9–486 nm a fit was possible. This is acceptable because the sloping edges of AlO vibrational transitions are very temperature sensitive [51]. The obtained temperature for the vapour phase on the basis of the AlO molecule was nearly constant at $T = 2550$ K.

In the wavelength range from 603–650 nm the CuO $A^2\Sigma-X^2\Pi$ system is not superimposed by any other line or band emission. Only the $A^2\Sigma-X^2\Pi_{3/2}$ subsystem was calculated and fitted to the experimental spectra (Figure 10). The $A^2\Sigma-X^2\Pi_{1/2}$ subsystem (615–625 nm and 640–650 nm) was not calculated. The determined temperature for the vapour phase on the basis of the CuO molecule was between 2500 K and 2750 K nearly constant over time and in good agreement with the temperature of the AlO molecule.

5 Conclusion

The combustion zone of Al/CuO thermite was investigated by emission spectroscopy in the wavelength range from $\lambda = 350$ nm (UV)– $\lambda = 2140$ nm (NIR). From radiation of hot surfaces, melt and particles in the NIR range, the continuum temperature can be determined by fitting with a grey body function. The grey body radiation is also visible in the UV/VIS range and again the continuum temperature is obtained from the measured spectrum. By an absolute calibration of the spectrometer sensitivity not only the continuum temperature but also the emissivity is calculated and therefore, the radiated energy at the measurement point can be calculated. For the example system of an Al/CuO thermite in the UV/VIS range, continuum temperatures between 3000 K and 1000 K are obtained which are in good agreement with the NIR continuum temperature. The determined emissivity is between 0.002 at the beginning up to 0.57 at the two peaks after 2.5 ms and 5 ms. In the UV/VIS range, band systems of diatomic molecules can be identified and the temperature of the vapour phase can be determined from their spectra. During combustion of Al/CuO thermite, AlO, Cu_2 and CuO were observed. For Cu_2 and CuO potential energy curves and for the first time the Franck-Condon factors were calculated from the diatomic constants given in the literature. With a fit of the calculated to the experimental spectra, the temperature of the vapour phase of the burning Al/CuO thermite was determined between $T = 2500$ K and 2750 K for both diatomic molecules AlO and CuO. The results are in good agreement with the calculated adiabatic temperature of the stoichiometric thermite mixture of 19% Al and 81% CuO at $T_{\text{adiabatic}} = 2828$ K (Figure S2

in the supporting information). They were calculated with Ekvi System [52]. From these results, it seems that all diatomic molecules and therefore the whole vapour phase of the combustion process are in thermal equilibrium. In combination with the determined emissivity, these results would be interesting for modelling of thermite reactions and the elapsed radiation processes during thermite reactions.

Symbols and Abbreviations

A	Rotational constant of electron rotation
Al	Aluminium
AlO	Aluminium oxide
B_v	First rotational molecule constant
Cu_2	Copper dimer
CuO	Copper(II) oxide or the diatomic molecule
D_v	First centrifugal constant (second rotational molecule constant)
EKVI	Thermodynamic code
e	First rotational energy term by spin-splitting
F_v	Rotational energy
f	Second rotational energy term by spin-splitting
FWHM	Full-width half maximum
H_v	Second centrifugal constant (third rotational molecule constant)
I_k	Intensity [$W m^{-2} nm^{-1} sr^{-1}$]
J	Rotational quantum number
N_2	Nitrogen
NIR	Near infrared
P	Pressure [MPa]
P	Branch of the rotational energy with $\Delta J = -1$
Q	Branch of the rotational energy with $\Delta J = 0$
R	Branch of the rotational energy with $\Delta J = +1$
RKR	Rydberg-Klein-Rees method
S_J	Hönl-London factor dependent on the rotational quantum number
T	Temperature [K]
t	time [ms]
UV	Ultraviolet
VIS	Visible
Y	Coupling constant between Hund's case a and b
y_v	Measured value
$\Delta y_v, \Delta y_v$	Experimental error
z_v	Theoretical value
γ	Electron spin-rotation coupling constant
ε	Emissivity [-]
λ	Wavelength [μm] or [nm]
Λ	Projection of orbital angular momentum
v'	Vibrational quantum number excited state
v''	Vibrational quantum number ground state
χ^2	Chi-square function

The different states of the diatomic molecule are described by the energy level X (X = ground state, A = first excited state, B = second excited state, ...), the multiplicity s,

the projection of the orbital angular momentum Λ ($\Sigma = 0$, $\Pi = 1$, $\Delta = 2$, $\Phi = 3$, ...) and the total angular momentum $\Omega = |\Lambda + \Sigma|: \chi^{2s+1} \Lambda_{\Omega}$.

References

- [1] S. H. Fischer, M. C. Grubelich, Theoretical Energy Release of Thermites, Intermetallics and Combustible Metals, *24th International Pyrotechnics Seminar*, Monterey, California, USA, 27–31 July, **1998**.
- [2] H. Goldschmidt, C. Vautin, Aluminium as a Heating and Reducing Agent, *J. Soc. Chem. Ind. London* **1898**, 12, 543–545.
- [3] C. P. Lonsdale, Thermite Rail Welding: History, Process Developments, Current Practices and Outlook for the 21st Century, Conrail Technical Services Laboratory Altoona, PA 16601.
- [4] V. Sundaram, K. Logan, R. Speyer, Reaction path in the magnesium thermite reaction to synthesize titanium diboride, *J. Mater. Res.* **1997**, 12, 2657–2664, doi:10.1557/JMR.1997.0355.
- [5] H. X. Zhu, R. Abbaschian, In-situ processing of NiAl–alumina composites by thermite reaction, *Materials Science and Engineering: A*, **2000**, 282, Issues 1–2, 1–7, [https://doi.org/10.1016/S0921-5093\(99\)00788-1](https://doi.org/10.1016/S0921-5093(99)00788-1).
- [6] W.-J. Xi, N. Li, T. Zhang, W.-L. Zhu, H.-Z. Guo, Thermite reaction synthesis of nano-sized NiAl reinforced FeNiCr–TiC composite coating, *Journal of Alloys and Compounds* **2010**, 504, 414–417, <https://doi.org/10.1016/j.jallcom.2010.03.157>.
- [7] V. Ri, H. Nersisyan, S. Ch. Kwon, J. H. Lee, H.-Y. Suh, J.-G. Kim, A thermochemical and experimental study for the conversion of ilmenite sand into fine powders of titanium compounds, *Mater. Chem. Phys.* **2018**, 221, 1–10, <https://doi.org/10.1016/j.matchemphys.2018.09.031>.
- [8] L. L. Wang, Z. A. Munir, Y. M. Maximov, Review Thermite Reactions: their Utilization in the Synthesis and Processing of Materials, *J. Mater. Sci.* **1993**, 28, 3693–3708, <https://doi.org/10.1007/BF00353167>.
- [9] O. Odawara, J. Ikeuch, Vacuum Centrifugal-Thermite Process for Producing Ceramic-Lined Pipes, *J. Am. Ceram. Soc.* **1986**, 69, C-85–C-86, <https://doi.org/10.1111/j.1151-2916.1986.tb04761.x>.
- [10] M. Gaber Zaky, A. M. Abdalla, R. P. Sahu, I. K. Puri, M. Radwan, S. Elbasuney, Nanothermite colloids: A new prospective for enhanced performance, *Defence Technology* **2018**, <https://doi.org/10.1016/j.dt.2018.08.016>.
- [11] V. Weiser, E. Roth, S. Kelzenberg, W. Eckl, Pyrotechnic Incendiaries to Combat Toxic Clouds, *40th International Annual Conference of ICT*, June 24–26, **2009**, 13(1–12).
- [12] V. Baijot, L. Glavier, J. Ducéré, M. Djafari Rouhani, C. Rossi, A. Estève, Modeling the Pressure Generation in Aluminum-Based Thermite, *Propellants Explos. Pyrotech.* **2015**, 40, 402–412, <https://doi.org/10.1002/prop.201400297>.
- [13] L. Glavier, A. Nicolle, F. Jouot, B. Martin, J. Barberon, L. Renaud, C. Rossi, Nanothermite/RDX-Based Miniature Device for Impact Ignition of High Explosives, *Propellants Explos. Pyrotech.* **2017**, 42, 308–317, <https://doi.org/10.1002/prop.201600154>.
- [14] K. Monogarov, A. Pivkina, N. Muravyev, D. Meerov, D. Dilhan, Combustion of Micro- and Nanothermites under Elevating Pressure, *Physics Procedia* **2015**, 72, 362–365, <https://doi.org/10.1016/j.phpro.2015.09.111>.
- [15] M. L. Pantoya, J. J. Granier, Combustion Behavior of Highly Energetic Thermite: Nano versus Micron Composites, *Propellants Explos. Pyrotech.* **2005**, 30, 53–62, <https://doi.org/10.1002/prop.200400085>.

- [16] B. Khasainov, M. Comet, B. Veyssiere, D. Spitzer, Comparison of Performance of Fast-Reacting Nanothermites and Primary Explosives, *Propellants Explos. Pyrotech.* **2017**, *42*, 754–772, <https://doi.org/10.1002/prep.201600181>.
- [17] D. G. Piercey, T. M. Klapötke, Nanoscale Aluminum-Metal Oxide (Thermite) Reactions for Application in Energetic Materials, *Cent. Eur. J. Energ. Mater.* **2010**, *7*, 115–129.
- [18] P. Chandra Ray, H.-T. Yu, P. P. Fu, Toxicity and Environmental Risks of Nanomaterials: Challenges and Future Needs, *J. Environ. Sci. Health Part C* **2009**, *27*, 1–35, <https://doi.org/10.1080/10590500802708267>.
- [19] D. Meerov, D. Ivanov, K. Monogarov, N. Muravyev, A. Pivkina, Y. Frolov, Mechanical Activation of Al/MoO₃ Thermite as a Component of Energetic Condensed Systems to Increase Its Efficiency, *Cent. Eur. J. Energ. Mater.* **2009**, *6*, 277–289, .
- [20] A. N. Streletskii, I. V. Kolbanev, G. A. Vorobieva, A. Yu. Dolgoborodov, V. G. Kirilenko, B. D. Yankovskii, Kinetics of Mechanical Activation of Al/CuO Thermite, *J. Mater. Sci.* **2018**, *53*, 13550–13559, <https://doi.org/10.1007/s10853-018-2412-3>.
- [21] E.-C. Koch, A. Hahma, V. Weiser, E. Roth, S. Knapp, Metal-Fluorocarbon Pyrolants. XIII: High Performance Infrared Decoy Flare Compositions Based on MgB₂ and Mg₂Si and Polytetrafluoroethylene/Viton, *Propellants Explos. Pyrotech.* **2012**, *37*, 432–438, <https://doi.org/10.1002/prep.201200044>.
- [22] V. Weiser, E. Roth, A. Raab, M. Juez-Lorenzo, S. Kelzenberg, N. Eisenreich, Thermite Type Reactions of Different Metals with iron-Oxide and the Influence of Pressure, *Propellants Explos. Pyrotech.* **2010**, *35*, 240–247, <https://doi.org/10.1002/prep.201000024>.
- [23] M. R. Weismiller, J. G. Lee, R. A. Yetter, Temperature Measurements of Al Containing Nano-thermite Reactions using Multi-Wavelength Pyrometry, *Proc. Combust. Inst.* **2011**, *33*, 1933–1940, <https://doi.org/10.1016/j.proci.2010.06.094>.
- [24] K. Sullivan, M. Zachariah, Simultaneous Pressure and Optical Measurements of Nanoaluminum Thermites: Investigating the Reaction Mechanism, *J. Propul. Power* **2010**, *26*, 467–472, <https://doi.org/10.2514/1.45834>.
- [25] Yajing Peng, Yinghui Wang, B. Palpant, Xing He, Xianxu Zheng, Yanqiang Yang, Modeling Heat-Induced Chemical Reaction in Nanothermites Excited by Pulse Laser: a Hot-Spot-Model, *Int. J. Mod. Phys. B* **2010**, *24*, 381–395, <https://doi.org/10.1142/S0217979210055135>.
- [26] S. Kelzenberg, V. Weiser, E. Roth, N. Eisenreich, B. Berger, B. Haas, Hot Spot Modeling of Thermite Type Reactions Regarding Particle Size and Composition, *EuroPyro 2007 (9ième Congrès International de Pyrotechnie du GPTS) and the 34th International Pyrotechnics Seminar*, October 8th–11th, 2007, Beaune, France, Proceedings by GTPS (Groupe de Travail de Pyrotechnie, France and the International Pyrotechnics Society, **2007**, *1*, 81–796.
- [27] S. Knapp, V. Weiser, S. Kelzenberg, N. Eisenreich, Modeling Ignition and Thermal Wave Progression in Binary Granular Pyrotechnic Compositions, *Propellants Explos. Pyrotech.* **2014**, *39*, 423–433, <https://doi.org/10.1002/prep.201400023>.
- [28] V. Weiser, E. Roth, A. Raab, S. Kelzenberg, S. Knapp, W. Eckl, Combustion of Fuel Particles (Al, B, Mg, Si, Ti, Zr) in Combination with RDX and the Influence of Additional Air, *Europyro2011*, Reims, France, May 16–19, **2011**.
- [29] W. Eckl, N. Eisenreich, W. Liehmann, H. Schneider, V. Weiser in *Non-Intrusive Combustion Diagnostics*, (Eds. K. K. Kuo, T. P. Parr), Begell House Inc. New York, **1994**, pp. 253..
- [30] V. Weiser, N. Eisenreich, Fast Emission Spectroscopy for a Better Understanding of Pyrotechnic Combustion Behaviour, *Propellants Explos. Pyrotech.* **2005**, *30*, 67–78, <https://doi.org/10.1002/prep.200400087>.
- [31] R. W. B. Pearse, A. G. Gaydon, The identification of molecular spectra, Fourth Edition, *Chapman and Hall Ltd.*, London, **1976**.
- [32] W. Demtröder, *Molekülphysik*, Oldenbourg Wissenschaftsverlag GmbH, **2003**.
- [33] G. Herzberg, The spectra and structures of simple free radicals: an introduction to molecular spectroscopy, *Courier Corporation*, **1971**.
- [34] J. A. Coxon, S. Naxakis, Rotational Analysis of the B²Σ⁺-X²Σ⁺ System of the Aluminium Monoxide Radical, AlO, *J. Mol. Spectrosc.* **1985**, *111*, 102–113, [https://doi.org/10.1016/0022-2852\(85\)90073-6](https://doi.org/10.1016/0022-2852(85)90073-6).
- [35] M. D. Saksena, M. N. Deo, K. Sunanda, S. H. Behere, C. T. Londhe, Fourier Transform Spectral Study of B²Σ⁺-X²Σ⁺ System of AlO, *J. Mol. Spectrosc.* **2008**, *247*, 47–56, <https://doi.org/10.1016/j.jms.2007.10.002>.
- [36] M. D. Saksena, G. S. Ghodgaonkar, M. Singh, The B²Σ⁺-X²Σ⁺ system of AlO, *J. Phys. B: At. Mol. Opt. Phys.* **1989**, *22*, 1993–1996, <https://doi.org/10.1088/0953-4075/22/12/014>.
- [37] M. Singh, J. P. Chaturvedi, Some Vibrational Bands of B-X System of AlO Molecule in the Sun Spectra, *Bull. Astron. Soc. India* **1986**, *14*, 175–179.
- [38] I. Kovacs, Rotational Structure in the Spectra of Diatomic Molecules, *Adam Hilger Ltd.*, London, **1969**.
- [39] R. J. M. Bennett, Hönl-London factors for doublet transitions in diatomic molecules, *Mon. Not. R. Astron. Soc.* **1970**, *147*, 35–46.
- [40] A. Schadee, The formation of molecular lines in the solar spectrum, B. A. N. *Astronomical Institutes of the Netherlands* **1964**, *5*, 311–357.
- [41] E. Hill, J. H. Van Vleck, On the quantum mechanics of the rotational distortion of multiplets in molecular spectra, *Phys. Rev.* **1928**, *32*, 250, <https://link.aps.org/doi/10.1103/PhysRev.32.250>.
- [42] O. Appelblad, A. Lagerqvist, The Spectrum of CuO: Rotational Analysis of Some Blue and Red Bands, *Phys. Scr.* **1974**, *10*, 307–324, <https://doi.org/10.1088/0031-8949/10/6/007>.
- [43] R. H. Page, C. S. Gudeman, Rotationally resolved dicopper (Cu₂) laser-induced fluorescence spectra, *J. Chem. Phys.* **1991**, *94*, 39–51, <https://doi.org/10.1063/1.460355>.
- [44] J. in Jin, Q. Ran, X.-P. Zhang, Y. Chen, C.-X. Chen, Investigation of the A²Σ⁺ state of CuO by laser-induced fluorescence, *Chinese Physics* **2002**, *11*, 5, 481–485, <https://doi.org/10.1088/1009-1963/11/5/313>.
- [45] R. J. Le Roy, RKR 2.0: A Computer Program Implementing the First-Order RKR Method for Determining Diatomic Molecule Potential Energy Curves, *University of Waterloo Chemical Physics Research Report CP-657R*, see <http://leroy.uwaterloo.ca>, **2004**.
- [46] S. M. Kirschner, J. K. G. Watson, RKR Potentials and Semi-classical Centrifugal Constants of Diatomic Molecules, *J. Mol. Spectrosc.* **1973**, *47*, 234–242, [https://doi.org/10.1016/0022-2852\(73\)90007-6](https://doi.org/10.1016/0022-2852(73)90007-6).
- [47] A. Daoudi, J. Touimi Benjelloun, P. Flament, G. Berthier, Potential Energy Curves and Electronic Structure of Copper Nitrides CuN and CuN⁺ versus CuO and CuO⁺, *J. Mol. Spec.* **1999**, *194*, 8–16, <https://doi.org/10.1006/jmsp.1998.7596>.
- [48] R. J. Le Roy, LEVEL 8.0: A Computer Program for Solving the Radial Schrödinger Equation for Bound and Quasibound Levels, *University of Waterloo Chemical Physics Research Report CP-663*, **2007**, see <http://leroy.uwaterloo.ca/programs>.
- [49] M. J. D. Powell, A method for minimizing a sum of squares of non-linear functions without calculating derivatives, *The Computer Journal* **1965**, *7*, 303–307, <https://doi.org/10.1093/comjnl/7.4.303>.

- [50] K. P. Huber, G. Herzberg, *Molecular Spectra and Molecular Structure: IV Constants of Diatomic Molecules*. Van Nostrand Reinhold Company, New York, **1979**, <https://doi.org/10.1007/978-1-4757-0961-2>.
- [51] S. Knapp, W. Eckl, S. Kelzenberg, A. Koleczko, A. Raab, E. Roth, S. Steinert, V. Weiser, *Emission Spectroscopy on Wire Explosions in Different Atmospheres, Proceedings of the HEMs 2011*, La Rochelle, France, **2011**.
- [52] B. Nöläng, Ekvi System 3.2, *BeN Systems*, Bålänge, Sweden, **2004**.

Manuscript received: July 27, 2018
Revised manuscript received: November 8, 2018
Version of record online: December 20, 2018